THE ASTROPHYSICAL JOURNAL, 422:243–247, 1994 February 10

A BROAD-BAND X-RAY TELESCOPE OBSERVATION OF THE BLACK HOLE CANDIDATE LMC X-1

ERIC M. SCHLEGEL,[1,2] F. E. MARSHALL, R. F. MUSHOTZKY, A. P. SMALE,[1,2] K. A. WEAVER,[3] P. J. SERLEMITSOS, R. PETRE, AND K. M. JAHODA
Code 666, Laboratory for High Energy Astrophysics, NASA/Goddard Space Flight Center, Greenbelt, MD 20771
Received 1993 June 28; accepted 1993 August 23

ABSTRACT

We present the spectrum of the black hole candidate LMC X-1 as observed by the Broad-Band X-ray Telescope. The spectrum cannot be fitted by a simple model, but it requires a soft disk blackbody component and a power-law tail, confirming earlier studies. The blackbody disk component is essentially unchanged since the *Ginga* measurement in 1987. The implied mass of the compact object is $\sim 4.7 \sqrt{\cos i}\, M_\odot$ from the soft component fit. We report a 95% confidence detection of weak emission features at ~ 5.1 keV and ~ 7.3 keV. If the 5.1 keV feature is attributed to Fe I Kα at 6.39 keV, then the redshift is ~ 0.19. No quasi-periodic behavior is found in the data at this epoch.

Subject headings: black hole physics — stars: individual (LMC X-1) — X-rays: stars

1. INTRODUCTION

LMC X-1, the first identified X-ray source in the LMC (Johnston, Bradt, & Doxsey 1979), is a black hole candidate (BHC). The X-ray spectrum cannot be fitted by a single-component model, but it requires at least two components: an ultrasoft blackbody with $kT \sim 0.8$ keV and a hard power law with a photon index of ~ 2.5 (Ebisawa et al. 1989). A quasi-periodic oscillation (QPO) of 0.075 Hz was discovered in *Ginga* data (Ebisawa et al. 1989), apparently associated with the hard spectral component. As first suggested by White & Marshall (1984), and verified by Ebisawa (1991), the ultrasoft component appears to be a characteristic unique to BHCs. Theoretically, this is expected, as a general relativistic accretion disk has a lower blackbody temperature than its Newtonian counterpart (Hanawa 1989; Fu & Taam 1990). However, more observational evidence is needed to confirm this inference, such as firm measures of the masses of the stars comprising the binary. The optical counterpart of LMC X-1 is still not firmly established (Cowley 1991), although the identification was strengthened by the discovery of a highly ionized He III nebula which is almost certainly an X-ray photoionized nebula (Pakull & Angebault 1986). Optical spectroscopy establishes the probable counterpart as an O7 binary with an orbital period of ~ 4 days, yielding a lower mass limit for the compact object of $\sim 2.6\ M_\odot$ (Hutchings, Crampton, & Cowley 1983). This lower limit is larger than the theoretical upper mass limit for a neutron star of $\sim 2.5\ M_\odot$ (e.g., Shapiro & Teukolsky 1983). A recent review of BHCs is available in Inoue (1991).

We describe here the X-ray spectral observation of LMC X-1 made using the Broad Band X-Ray Telescope (BBXRT).

2. BBXRT OBSERVATIONS

The Broad Band X-Ray Telescope (Serlemitsos et al. 1992) flew on the shuttle Columbia as one component of the multi-telescope Astro-1 mission. The flight of BBXRT was the first use of an X-ray detector with moderate energy resolution (~ 90 eV at 1 keV and ~ 160 eV at 6 keV) and a broad spectral coverage (0.3–12 keV). BBXRT was designed and built at GSFC by a team led by principal investigator Peter Serlemitsos (Serlemitsos et al. 1992). It consists of two co-aligned telescopes of 3.8 m focal length. The mirrors are thin, nested, gold-coated aluminum foils, with an effective area of ~ 150 cm^2 at 2 keV and 80 cm^2 at 7 keV for each telescope/detector combination. The mirrors focus the X-rays onto cooled, lithium-drifted silicon, solid state spectrometers. The spectrometers consist of 5 pixels per detector, 512 energy channels per pixel, with the central pixel having a 4.5 field of view. The overall field-of-view is 17′. The pixels are separated by a mask 1.5 across. The detector backgrounds are low, with ~ 0.02 counts s^{-1} in the central pixel and ~ 0.1 counts s^{-1} in the outer pixels.

Attempts to point at LMC X-1 were made on five occasions during the 9 day mission, but, unfortunately, none with on-axis pointings. Table 1 summarizes the pointings. With relatively large off-axis angles and a point-spread function with $\sim 1'$ FWHM, most photons were detected in an outer pixel. We lose little information by considering only the most populated pixels in our analysis (Table 1). This approach is justified by the rather high count rate from LMC X-1 (~ 15–18 counts s^{-1}) and the low total background (typically 0.5–0.8 counts s^{-1}). With these considerations, we have 6 pixels from three pointings. Unfortunately, only 2 or 3 pixels have relatively good signal-to-noise ratios strongly constraining our conclusions.

The target points were all made outside of the South Atlantic Anomaly, but the data were for the most part obtained during shuttle daylight (Sun angles $\sim 90°$ and Earth angles $\sim 90°$–$95°$). We used a daytime background spectrum from numerous daytime pointings when the two-axis pointer had drifted from its target. This background was scaled by the guard rate for the particular observation segment and then subtracted from the data. Weaver (1993) has shown that this process removes the background to rather high accuracy across the entire bandpass. Some residual background contamination exists below ~ 0.6 keV. Given the moderate column to LMC X-1 ($\sim 0.5 \times 10^{22}$ cm^{-2}) (Ebisawa 1991),

[1] Also, Universities Space Research Association.
[2] Postal address: Code 668, Laboratory for High Energy Astrophysics, NASA/Goddard Space Flight Center, Greenbelt, MD 20771.
[3] Also, University of Maryland.

TABLE 1

OBSERVATION JOURNAL

Pointing	Start Stop (MET[a])	Usable Exposure	Pixels Used[b]	Photon Fraction[c]	Off-Axis Angle	Aspect Solution	Approximate Count Rate
1	2^d 0:34:31 2^d 0:40:15	~345 s	...	...	~2°	Yes	~0.5
2	3^d 12:20:37 3^d 12:47:43	~1640 s	...	...	~1°	No	~0.2
3	3^d 18:47:19 3^d 18:57:19	~600 s	A4, B2[e]	83%	~3'.6[f]	No	~12, ~6
4	4^d 14:40:47 4^d 15:01:35	~1240 s	A1,[e] B3[e]	80%	~2'.4[f]	No	~11, ~9
5	5^d 11:08:39 5^d 11:57:03	~470 s	A3, B1	81%	~3'.5	No	~20, ~14

[a] MET is the mission elapsed time; 0^d 0:0:0 = 1990 December 2, 06:49:01 UT.
[b] Pixels used in continuum spectral fitting.
[c] Percentage of photons contained in pixels used of detected photons in all pixels.
[e] Pixels used to fit narrow, linelike features.
[f] Off-axis angle estimated by ray-tracing of BBXRT optics.

there is little detected source flux below ~0.7 keV, so no information is lost by ignoring those channels containing the residual contamination. Off-axis angles were estimated by ray-tracing, as aspect solutions did not exist.

3. RESULTS

Figure 1 presents the observed spectrum and fitted model of 1 pixel for clarity only. Spectral fitting was done using the BBXRT response matrix calibration (Weaver 1993) in which fits to spectra of the Crab Nebula show broad, ~3% amplitude residuals remaining, plus ~7% residuals at ~1.38 keV and the gold M edge at ~2.2 keV. A single-component model does not describe the observed LMC X-1 spectrum, but two-component models do. The best-fit model is a "multicolor blackbody disk" (Pringle 1981; Mitsuda et al. 1984) plus a power-law tail. All models fitted to the data are included in Table 2. The fitted column is 5.8×10^{21} cm^{-2}, matching previous measurements (White & Marshall 1984; Ebisawa et al. 1989). The power law photon index is 2.18 ± 0.37, in line with the apparently typical values of ~2.3–2.8 from previous missions (Ebisawa et al. 1989; White & Marshall 1984). The temperature of the disk blackbody is measured to be 0.83 ± 0.07 keV and appears relatively constant from the *Ginga* measurements made in 1987 ($kT \sim 0.19$ keV) (Ebisawa et al. 1989).

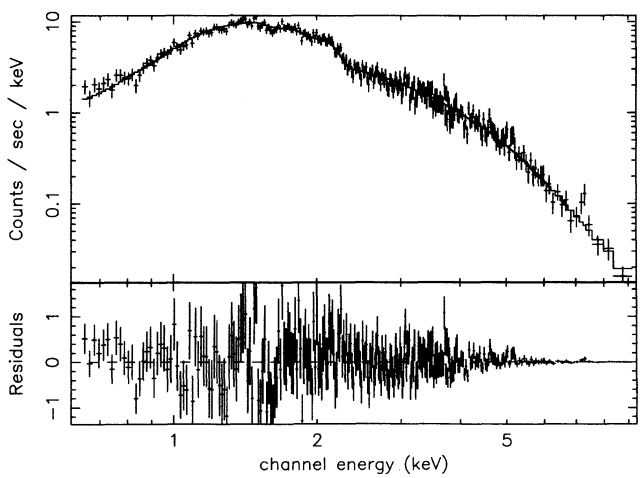

FIG. 1.—BBXRT spectrum (log flux scale) and residuals (linear scale) of the fit to LMC X-1. We show the data for only one pixel (pointing 4, pixel B3) for clarity, but the model fit was determined by a simultaneous fit to 6 pixels, with only the model normalization varying between pixels.

Fluorescent lines are expected from an accretion disk surrounding a black hole (e.g., Kojima & Fukue 1992; Matt, Fabian, & Ross 1993). The line should show the double-horn shape characteristic of accretion disks, with the lower energy horn small relative to the higher energy horn. Alternatively, infalling matter could be illuminated, producing an emission line. Ebisawa et al. (1989) found a line of equivalent width ~75 eV at 6.8 ± 0.2 keV in the 1987 July *Ginga* data. No iron line is apparent in the 6.5 keV region in the residuals of Figure 1. Attempts to fit a line proved fruitless, as the "fits" were zero width lines to single, high channels. A formal upper limit was assigned using the following approach. The best-fit continuum model was determined, and the fit parameters were frozen.[4] A Gaussian component was added to simulate an iron emission line in the 6.5 keV region, with a range of physical line widths (0 eV, 200 eV, 600 eV, 1000 eV). The line energy was then stepped from 6.2 to 7.0 keV in 0.1 keV increments. The individual pixels' line normalizations were held fixed relative to each other in the same ratio as their continuum normalizations. Then, for each physical line width and line energy, the absolute normalization was varied until χ^2 increased by +6.63 (99% significance for one parameter of interest). The equivalent width of the line was then calculated. Note that no fitting is being done, as the line energy and width are determined. The absolute normalization is the only free parameter. The results are plotted in Figure 2 for the range of physical line widths chosen. From Figure 2, the upper bound is certainly affected by the poor axial position of LMC X-1 on the detector and the limited exposure times. The upper limit is generally, however, below values quoted in the literature (e.g., <400 eV, White & Marshall 1984). The 0 eV upper limit curve suggests that a relatively narrow line of equivalent width <100 eV, similar to

[4] The correct approach allows the continuum parameters to vary. The good spectral resolution of the detector means that a weak line has little or no effect on the continuum parameter values.

TABLE 2

FORMAL FITS TO BINNED LMC X-1 SPECTRUM

Model	$(\chi^2/\nu)^a$	N_{par}	$N_H{}^b$ (10^{22} cm^{-2})	Parameter 1[b]	Parameter 2[b]
Power law[c]	1.906	8	1.17 ± 0.11	$\Gamma = 3.29 \pm 0.24$	...
Blackbody	1.774	8	0.23 ± 0.07	$kT = 0.61 \pm 0.08$	...
Bremsstrahlung	1.331	8	0.74 ± 0.08	$kT = 1.82 \pm 0.12$	...
Power law[c] + blackbody	1.274	15	0.59 ± 0.08	$\Gamma = 2.59 \pm 0.26$	$kT = 0.55 \pm 0.09$
Power law + blackbody disk	1.023	15	0.579 ± 0.09	$\Gamma = 2.18 \pm 0.37$	$kT = 0.83 \pm 0.07$
Ginga: Power law[cd] + blackbody disk	0.82	...	$0.50^{+0.13}_{-0.22}$	$\Gamma = 2.75 \pm 0.22$	$kT = 0.83 \pm 0.03$

[a] A total of 6 pixels were used for the continuum fits. The original number of degrees of freedom, for all models, was 1567. From this number must be subtracted the number of degrees of freedom N_{par} used in the model and listed above.
[b] The error bars are 90% for one parameter of interest.
[c] For the power-law model, Γ is the photon index.
[d] *Ginga* data, 1987 July, from Ebisawa 1991.

the Fe Kα lines observed in Cyg X-1 (equivalent width $\sim$44 eV) (Done et al. 1992; Marshall et al. 1993), could easily be present around 6.4 keV. A long, stable observation using a higher resolution instrument [e.g., the CCD spectrometers on *ASCA* (*Astro* D)] will be necessary to establish the existence of any lines in this region.

Data from *Ginga* (Ebisawa 1991) have shown the presence of a broad, shallow absorption-like feature in the 7–10 keV region. It is believed that this feature is related to the iron K-edge, and is produced by reflection of X-rays by optically thick matter (such as the accretion disk). The edge energy was shown to vary from 6.9 to 8.4 keV using a "smeared" edge model (Ebisawa 1991). The decreasing effective area of the BBXRT detectors at higher energies prevents any fits to this component, as the data are unfortunately of sufficiently poor signal-to-noise ratio to detect any features in the residuals of the power law-fit. The BBXRT upper limit on the equivalent width of the edge is $\sim$0.5 keV, but the errors are large.

Ebisawa et al. (1989) discovered a 0.075 Hz QPO in a segment of their *Ginga* data. The QPO was present in 1987 April but was not present in data obtained three months later. The QPO was apparently associated with the hard spectral component, as that component changed its behavior between the two observation epochs, while the behavior of the soft blackbody disk component was nearly constant over the same interval. We computed the power spectral density for only one segment (number 4) of the BBXRT data to search for any QPO activity. The power spectrum was flat. The power spectrum was fitted with a power law, for the continuum, and a Gaussian component to simulate the QPO. The strength of the line was then increased until $\Delta\chi^2$ went up by 2.71 (90%) and 6.63 (99%). The resulting signal strengths were 1.2% and 1.6%, which are $\sim$8.5 σ and $\sim$6.4 σ lower than the signal found by Ebisawa et al. We interpret these values to mean that no QPO or periodic behavior was found at any frequency between 0.01 and 4 Hz.

Finally, we turn to the possible detection of two small emission-like features present at $\sim$5.1 keV and $\sim$7.3 keV. Figure 3 shows an expanded view of the data and the model in the 4.6 to 7.6 keV region, again showing only 1 pixel for clarity. Note that the features are residuals from the continuum fit and are not the data divided by a model, a presentation method

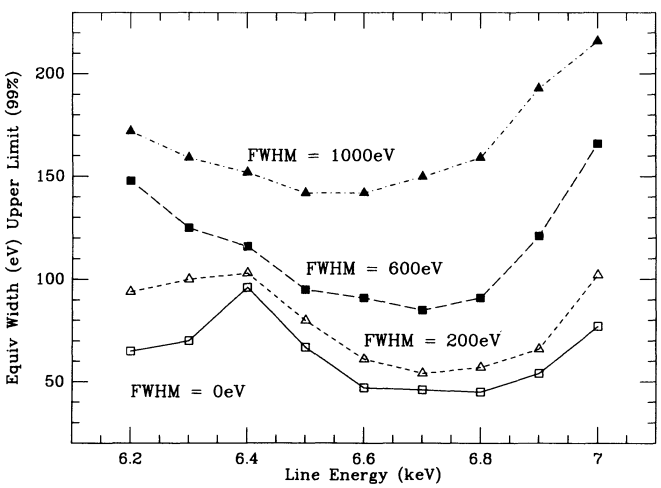

FIG. 2.—Upper limits on the equivalent width of an iron emission line in the 6.5 keV region for various physical line widths. See § 3 of the text for the details.

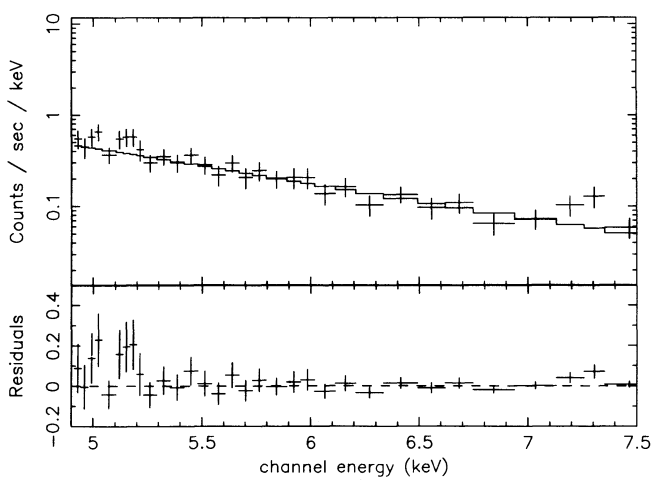

FIG. 3.—Expanded version of Fig. 1. Note the line features at $\sim$5.1 keV and $\sim$7.3 keV. Also note that the flux scale is linear.

often used to emphasize weak features. These linelike features are present in the three pixels with the highest signal-to-noise ratio. The features are admittedly not strong and are narrow, being consistent with a zero-width line broadened by the finite energy resolution of the BBXRT detectors. Assuming that the features are emission lines, we used Gaussians to fit the lines in the 3 pixels. We chose to ignore the noisy and less well-exposed pixels on the grounds that poor statistics do not aid the identification of a weak, narrow feature. Recall that we are using 1 pixel from each of the long data segments, so the feature is present on more than 1 day of the mission.

The fit was done using a zero-width line, and the line energy and normalization were free parameters. The pixels were all held fixed relative to each other in the same ratio as the continuum normalizations. The fitted line energies are 5.13 ± 0.06 keV (90% error) and 7.31 ± 0.09 keV, with equivalent widths of ~ 60 eV. We cannot claim unambiguously to detect these lines, as they are only significant at the 95% level (unfortunately). χ^2 dropped by ~ 6.4 from the minimum continuum fit, while a decrease of 6.17 is necessary for 95% significance for two parameters of interest (line energy and an absolute pixel normalization). We remain confident these features are not instrumental because nothing similar is present in the BBXRT Crab Nebula spectrum, nor in the data of the binary X-ray pulsar X Per (Schlegel et al. 1993), nor Cyg X-2 or Cyg X-3 (Smale et al. 1993a, 1993b, respectively). There are no known X-ray emission lines from abundant elements in this energy region (Kortright 1986). The features do not match the impressiveness of the broad, redshifted iron line in *EXOSAT* data on the BHC Cyg X-1 (Barr, White, & Page 1985) or the broad (2.7 keV FWHM), redshifted iron Kα line present at ~ 5.9 keV in the *EXOSAT* data of the soft X-ray transient 4U 1543−47 (van der Woerd, White, & Kahn 1989), or the line detections in SS 433 (Watson et al. 1986; Matsuoka, Takano, & Makishima 1986).

If the features are real, two possibilities emerge. First, the lines could be unrelated, in which case the 5.1 keV line could be the redshifted Fe I Kα 6.39 keV line. The calculated redshift is ~ 0.19, with higher redshifts resulting from choices of more highly ionized species of iron. Second, we could attribute the features to an iron Kα line from an X-ray photoionized accretion disk as in Matt, Fabian, & Ross (1993). In their Figure 6, for an extended source geometry, a double-horned line profile results for an inclination angle of 70°. The redshifted horn is present at about 5 keV, and the blueshifted horn is present at ~ 7.3 keV. The observed fluxes in the two lines are approximately equal, as opposed to the models which show the blueshifted horn to be the stronger component. A crude simulation using the BBXRT response matrix shows that even though the effective area is decreasing above 6 keV, the decline is probably not so steep as to invert the red-blue asymmetry sufficient. An *ASCA* observation should provide better quality data to confirm the presence of the lines and to study the potential asymmetry.

4. DISCUSSION

The multicolor disk blackbody (Pringle 1981; Mitsuda et al. 1984) is quite successful in describing the soft behavior of the BHCs. The continuum fit parameters are essentially unchanged from those determined by Ebisawa (1991) with *Ginga* data obtained in 1987. In particular, the temperature of the ultrasoft component appears to be measured rather accurately at 0.83 keV. The *Ginga* fitted value was 0.91 keV in 1987 July. The power-law component may be slightly harder than in the *Ginga* data; however, the error bar is sufficiently large that the *Ginga* values are within 2 σ of the value measured here. Variations in the hardness of the power-law tail are known to occur. For example, Makishima et al. (1986) noted the variations in the hard power law photon index in their study of the BHC GX 339−4, where the tail varied in index from −0.9 to −2.1 over approximately a 5 day interval. The typically poor temporal coverage by X-ray satellites as yet prevents detailed understanding of the causes of the variations.

Ebisawa (1991) found broad, edgelike absorption features in the five BHCs observed by *Ginga*. Such a feature was present at about 25% of the model continuum in the 1987 April *Ginga* data of LMC X-1. Given the decreasing effective area of the BBXRT detectors above ~ 7 keV, we cannot confirm the presence of the broad absorption features. However, if the broad edgelike feature *is* an edge, then we expect the presence of a fluorescence line, due to reflection, at about 6.4 keV. We have set firm upper limits on the presence of a line in the 6.5 keV region at the observation epoch. The lack of a line suggests that it may be variable in strength, being somewhat weaker at the BBXRT epoch. We have not done a simulation to see at what level the line must vary to remain undetected in the BBXRT observation, but we suspect that a somewhat small variation is all that is required.

Table 3 lists a few derived values for the black hole mass, the mass accretion rate, and the luminosity for LMC X-1. We also include values from the BHC GX 339−4 (Makishima et al. 1986) and LMC X-1 from Ebisawa (1991) for comparison. The values have been derived from the following. The form for the normalization of the blackbody accretion disk model is $r_{\rm in}\sqrt{\cos i}$, where $r_{\rm in}$ is the radius of the inner edge of the accretion disk, and i is the system inclination (Ebisawa et al. 1991). We equate this to the Schwarzschild radius r_S, yielding a mass estimate. The luminosity of the disk component is estimated from $L_X = 4\pi r_{\rm in}^2 \sigma T_{\rm in}^4$, where the symbols have their usual meaning. We have assumed a distance to LMC X-1 of 50 kpc. The mass accretion rate can be estimated from $L = g^2 M\dot{M}/2r_{\rm in}$, where $g^2 = \sqrt{1 - (r_S/r)}$ is the general relativistic correction. Better values should be available once LMC X-1 is observed with *ASCA*.

TABLE 3

DERIVED PARAMETERS FOR LMC X-1

Parameter	LMC X-1[a]	GX 339−4[b]	LMC X-1[c]
$M_{\rm BH}(M_\odot)$	$4.7\sqrt{\cos i}$	$2.3\sqrt{\cos i}$	$\sim 5.0\sqrt{\cos i}$
L (ergs s^{-1}) ..... (2–10 keV)	$1.0 \times 10^{38}/\cos i$	$4.3 \times 10^{37}/\cos i$	$\sim 1.22 \times 10^{38}/\cos i$
$\dot{M}(M_\odot\ {\rm yr}^{-1})$	$2.9 \times 10^{-8}/\cos i$	$3.7 \times 10^{-9}/\cos i$	$\sim 1.9 \times 10^{-8}/\cos i$

[a] Values derived from data in this paper.
[b] GX 339−4 values from Makishima et al. 1986.
[c] Values derived from 1987 July *Ginga* data (Ebisawa 1991).

REFERENCES

Barr, P., White, N. E., & Page, C. G. 1985, MNRAS, 216, 65P
Cowley, A. P. 1991, in Frontiers of X-Ray Astronomy, ed. Y. Tanaka & K. Koyama (Tokyo: Universal Academy), 344
Done, C., Mulchaey, J. S., Mushotzky, R. F., & Arnaud, K. A. 1992, ApJ, 395, 275
Ebisawa, K. 1991, Ph.D. thesis, Univ. Tokyo
Ebisawa, K., Mitsuda, K., & Hanawa, T. 1991, ApJ, 367, 213
Ebisawa, K., Mitsuda, K., & Inoue, H. 1989, PASJ, 41, 519
Fu, A., & Taam, R. 1990, ApJ, 349, 553
Hanawa, T. 1989, ApJ, 341, 948
Hutchings, J. B., Crampton, D., & Cowley, A. P. 1983, ApJ, 275, L43
Inoue, H. 1991, in Frontiers of X-Ray Astronomy, ed. Y. Tanaka & K. Koyama (Tokyo: Universal Academy), 291
Johnston, M. D., Bradt, H. V., & Doxsey, R. E. 1979, ApJ, 233, 514
Kojima, Y., & Fukue, J. 1992, MNRAS, 256, 679
Kortright, J. B. 1986, in X-Ray Data Booklet, ed. D. Vaughn (Berkeley: Lawrence Berkeley Lab.), 2
Makishima, K., et al. 1986, ApJ, 308, 635
Marshall, F. E., et al. 1993, ApJ, 419, 301
Matsuoka, M., Takano, S., & Makishima, K. 1986, MNRAS, 222, 605
Matt, G., Fabian, A. C., & Ross, R. R. 1993, MNRAS, 262, 179
Mitsuda, K., et al. 1984, PASJ, 36, 741
Pakull, M. W., & Angebault, L. P. 1986, Nature, 322, 511
Pringle, J. 1981, ARA&A, 19, 137
Schlegel, E. M., et al. 1993, ApJ, 407, 744
Serlemitsos, P. J., et al. 1992, in Proc. 28th Yamada Conf. on X-Ray Astronomy, ed. Y. Tanaka & K. Koyama (Tokyo: Universal Academy), 221
Shapiro, S., & Teukolsky, S. 1983, Black Holes, White Dwarfs, and Neutron Stars (New York: Wiley)
Smale, A. P., et al. 1993a, ApJ, 410, 796
Smale, A. P., Mushotzky, R. F., Schlegel, E. M., Weaver, K. A., Serlemitsos, P. J., Marshall, F. E., Petre, R., & Jahoda, K. 1993b, ApJ, 410, 000
van der Woerd, H., White, N. E., & Kahn, S. M. 1989, ApJ, 344, 320
Watson, M. G., Stewart, G. C., Brinkmann, W., & King, A. R. 1986, MNRAS, 222, 261
Weaver, K. A. 1993, Ph.D. thesis, Univ. of Maryland, in preparation
White, N. E., & Marshall, F. E. 1984, ApJ, 281, 354